ACS APPLIED MATERIALS & INTERFACES

Research Article

www.acsami.org

Angiogenesis in Bone Regeneration: Tailored Calcium Release in Hybrid Fibrous Scaffolds

Oscar Castaño,*[,†,‡,§] Nadège Sachot,[†,‡] Elena Xuriguera,[∥] Elisabeth Engel,[†,‡,§] Josep A. Planell,[†,‡,§] Jeong-Hui Park,[⊥,#] Guang-Zhen Jin,[⊥,#] Tae-Hyun Kim,[⊥,#] Joong-Hyun Kim,[⊥,#] and Hae-Won Kim[⊥,#]

[†]Biomaterials for Regenerative Therapies, Institute for Bioengineering of Catalonia (IBEC), 08028, Barcelona, Spain

[‡]CIBER de Bioingeniería, Biomateriales y Nanomedicina (CIBER-BBN), 08028 Barcelona, Spain

[§]Dpt. Materials Science and Metallurgical Engineering, Universitat Politècnica de Catalunya (UPC), 08028 Barcelona, Spain

[∥]Dpt. Materials Science and Metallurgical Engineering, Universitat de Barcelona (UB), 08028 Barcelona, Spain

[⊥]Institute of Tissue Regeneration Engineering (ITREN), Dankook University, 330-714 Cheonan, South Korea

[#]Dpt. Nanobiomedical Science & BK21 Plus NBM Global Research Center for Regenerative Medicine, Dankook University, 330-714 Cheonan, South Korea

Supporting Information

ABSTRACT: In bone regeneration, silicon-based calcium phosphate glasses (Bioglasses) have been widely used since the 1970s. However, they dissolve very slowly because of their high amount of Si (SiO_2 > 45%). Recently, our group has found that calcium ions released by the degradation of glasses in which the job of silicon is done by just 5% of TiO_2 are effective angiogenic promoters, because of their stimulation of a cell-membrane calcium sensing receptor (CaSR). Based on this, other focused tests on angiogenesis have found that Bioglasses also have the potential to be angiogenic promoters even with high contents of silicon (80%); however, their slow degradation is still a problem, as the levels of silicon cannot be decreased any lower than 45%. In this work, we propose a new generation of hybrid organically modified glasses, ormoglasses, that enable the levels of silicon to be reduced, therefore speeding up the degradation process. Using electrospinning as a faithful way to mimic the extracellular matrix (ECM), we successfully produced hybrid fibrous mats with three different contents of Si (40, 52, and 70%), and thus three different calcium ion release rates, using an ormoglass−polycaprolactone blend approach. These mats offered a good platform to evaluate different calcium release rates as osteogenic promoters in an in vivo subcutaneous environment. Complementary data were collected to complement Ca^{2+} release analysis, such as stiffness evaluation by AFM, ζ-potential, morphology evaluation by FESEM, proliferation and differentiation analysis, as well as in vivo subcutaneous implantations. Material and biological characterization suggested that compositions of organic/inorganic hybrid materials with a Si content equivalent to 40%, which were also those that released more calcium, were osteogenic. They also showed a greater ability to form blood vessels. These results suggest that Si-based ormoglasses can be considered an efficient tool for calcium release modulation, which could play a key role in the angiogenic promoting process.

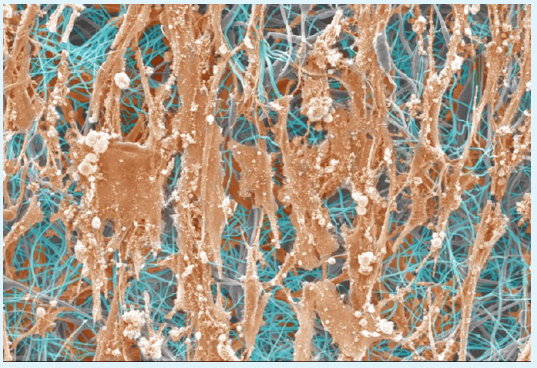

KEYWORDS: *angiogenesis, sol−gel, hybrid materials, ormoglasses, electrospinning*

1. INTRODUCTION

Calcium is a well-known osteoinductor promoter. Proliferation and differentiation of bone cells such as osteoblasts and osteoclasts, among others, are regulated by calcium-sensing receptor (CaSR).[1,2] Several previous in vivo studies indicated that bone marrow progenitor cells are recruited to high calcium concentration environments, suggesting a CaSR-mediated chemotaxis and a further bone resorption.[3,4] In fact, researchers have reported that the blocking of CaSR produced a decrease in ALP activity and expression of osteocalcin, as well as a significant reduced mineralization.[5]

Efficient osteogenesis cannot be feasible without an associated close vascularitzation (100−200 μm) of the construct, as cells need the supply of oxygen, nutrients, signaling, the elimination of their byproducts, and the recruiting of other cells.[6] Calcium has also been proposed as an angiogenic promoter by our group.[7] In this study, hybrid scaffolds containing a calcium phosphate glass doped with 5% TiO_2 triggered angiogenesis through mechanical and biochemical signaling synergistic pathways. The mechanosensitive pathway is upregulated by nonmuscle myosin II contraction. On the other hand, the biochemical signaling is controlled by

Received: February 11, 2014
Accepted: April 22, 2014
Published: April 22, 2014

Table 1. Nominal and Real Percentage Composition of the Hybrid Fibers with Their Average Thicknesses, Water Contact Angle, DMT Modulus, and RMS

	PCL-S40		PCL-S52		PCL-S70	
EDS composition	nom	real	nom	real	nom	real
Si	40.0	43.3 ± 2.5	52.0	50.3 ± 1.5	70.0	66.3 ± 1.7
Ca	50.0	45.5 ± 2.5	40.0	40.4 ± 1.9	25.0	28.3 ± 0.9
P_2	10.0	11.7 ± 0.1	8.0	9.3 ± 0.4	5.0	5.5 ± 0.7
⌀ (μm)	2.1 ± 0.4		1.9 ± 0.3		2.2 ± 0.3	
contact angle (deg)	33.6 ± 0.4		27.1 ± 2.3		20.9 ± 1.9	
DMT modulus (MPa)	64.4 ± 2.7		33.7 ± 1.1		18.8 ± 0.2	
RMS (nm)	5.5 ± 0.5		7.0 ± 1.0		7.7 ± 0.6	

the CaSR. Both signals trigger a synergistic effect by the activation of endothelial progenitor cells (EPCs)-mediated vascular endothelial growth factor (VEGF) and VEGF receptor 2 (VEGFR-2) expression, which promote progenitor cell homing, differentiation and tubulogenesis.

In recent years, many approaches have been considered for the development of bioactive materials and technical methods targeted for use in tissue regeneration as scaffolds for bone healing and microenvironment mediators.[8] Most of the developed materials have combined a polymer matrix, which supports the mechanical stability of the construct, and a bioactive ceramic or glass.[9−13] One of the more promising bioactive candidates used as bioactive constituent in composite materials are silicon based glasses such as Bioglasses. Bioglasses are inorganic glasses with a SiO_2-based backbone that also include CaO and P_2O_5 in their formulations with a bioactive minimum Si content (in the form of SiO_2) 45%,[14] with efficient osteogenesis capacity but poor degradation[15] compared with Ti-based glasses.[16] Recently, some studies propose Bioglasses, with a Si content between 60 and 80% as angiogenic promoters due to their controlled Ca^{2+} release.[17]

However, an important issue has appeared due to different degradation rates between the composite components and lack of surface cohesion,[18,19] which unfortunately can provoke the release of one of the domains unilaterally, that is, particles, to the bloodstream. That can happen in composites whose constituents are only linked by weak forces; thus, a covalent or ionic bond is required, especially when the release of key agents is involved.[20] As a consequence, this is a major challenge in the field of hybrid biomaterials, and several studies have evaluated the possibility of functionalizing inorganic particles in order to create a better union between the phases. For example, surfactants can be used to wet the polymer[21] or a covalent bonding can be created to attach the bioactive coating on the surface of the biodegradable polymer in order to directly expose the bioactive component to the cell, as was recently reported by our group.[22] On the other hand, this challenge can also be overcome if the two domains involved in the graft are of similar nature: organic, as well as with good surface affinity and interaction. Several positive studies have been made up to now using a combination of gelatin and siloxane for bone regeneration, where the lack of calcium in the composition meant that a prior mineralization became necessary by rinsing the nanofibers in a $CaCl_2$ solution.[23]

Electrospinning is a technique that has recently gained widespread interest due to its efficiency in producing nanostructured fibers to create an artificial extracellular matrix; in other words, it establishes a perfect starting point for cell adhesion, and thus proliferation and differentiation.[24] As a general requirement, electrospun fibers, which usually range from tens of nanometers to a few micrometers in diameter, should be biocompatible, be physiologically degradable, and able to be metabolized. Consequently, there will be a gradual release of byproducts to the bloodstream.

Considering this and with the aim to be able to modulate calcium release from a biomaterial, in this work, we have evaluated the possibility of producing high soluble blends of organometallic-modified amorphous networks (ormoglasses) and a biodegradable polymer to control calcium release through the modification of the chemical composition. Sol−gel method was selected to develop the organometallic network by means of alkoxide precursors in an inert atmosphere through a partial hydrolysis and condensation process; ε-polycaprolactone (PCL) was selected as the biodegradable polymer. Hence, the final aim was to join both domains at a nanometric level to obtain a tuned ion-agent release and controlled degradation in order to act as cell homing and enhance osteogenesis. Special attention was paid in the bulk, interface and degradation properties, which were evaluated by FE-SEM, EDS, DSC, TGA, tensile-strain assays, pH and Ca^{2+} release evaluation, contact angle measurements, AFM, and ζ-potential. We also performed cell proliferation assays, ALP, Western blotting analysis, and PCR in vitro test analysis. Finally, we performed in vivo subcutaneous tests to evaluate the biocompatibility and the osteogenic potential. However, results were surprisingly positive when we evaluated the possibility of the promotion of angiogenesis correlated to the calcium release tuning.

2. MATERIALS AND METHODS

2.1. Precursor Solution. Precursor solutions using metal alkoxides were prepared in an inert atmosphere as follows: while metallic Calcium (Sigma-Aldrich 99%) was refluxed in anhydrous 2-methoxyethanol (Sigma-Aldrich 99%), phosphorus precursor solution was obtained from a reflux of P_2O_5 (Sigma-Aldrich 97%) in absolute ethanol (Sigma-Aldrich >99%). Silicon precursor solution was commercially acquired as tetraethylorthosilicate (TEOS, Aldrich, 98%). The final precursor solution was prepared by homogeneously mixing the different single precursor solutions in their appropriate molar ratio. Once the final solution was ready, a water volume (Si/H_2O = 1:3 molar ratio) was added in order to achieve a partial gelation and produce a viscous ORMOGLASS sol after 30 s of vigorous stirring (for more details, see Scheme S1 in the Supporting Information). Based on a previous work by Kim et al.,[25] which considered a constant relation of Ca/P = 5, three contents of Si were tested (Table 1). In parallel, a solution of 16% w/w polycaprolactone (PCL, Sigma-Aldrich, MW = 70 000−90 000 kDa) in tetrahydrofuran (THF, Sigma-Aldrich, 99%) was prepared. Then a 20% v/v partially gelated ORMOGLASS sol was added to the PCL solution with vigorous stirring in order to obtain an electrospinnable slurry (see resultant viscosities in Table S1 in the Supporting Information).

Slurries were finally electrospun using a conventional setup with a grounded flat collector to achieve randomly distributed fiber sheets.

The applied voltage was 12 kV, a solution feed of 1 mL·h^{-1}, and a distance tip-collector of 15 cm.

2.2. Viscosity Measurements. Viscosity was evaluated using a vibrational viscosimeter SV-10 (AND Company, limited, Japan). We immersed the gold-plate sensor plate in 10 mL of electrospinnable solution in a quartz recipient surrounded by a water jacket. All the measurements were evaluated at 23.1 ± 0.3 °C.

2.3. FE-SEM, EDS Analysis, and Thickness Measurement. Field emission scanning electron microscopy (FESEM) and energy dispersive spectrometry (EDS or EDAX) analysis were made on FEI nova nanoSEM FESEM (Nova-Nano SEM-230; FEI Co., The Netherlands) and Quanta 200 SEM (Quanta 200 XTE 325/D8395; FEI Co., The Netherlands) instruments, respectively. It allowed the assessment of the microstructure of the samples, which were previously covered with a layer of carbon to be electron conductive. Energy dispersive spectrometry allowed the quantification of the chemical composition of the samples.

The thickness of the fibers was also measured using SEM images assisted with imageJ[26] open source software. Twenty-five fibers were randomly selected, and then average mean size and standard deviation were calculated.

2.4. Thermal Analysis. Fibrous scaffolds were characterized by differential scanning calorimetry (DSC, Q-20, TA Instruments, New Castle, DE). Samples of approximately 5 mg were placed in aluminum crucibles under a nitrogen atmosphere and heated from 20 °C up to 100 °C at a rate of 10 °C/min. The degree of crystallinity of PCL was assessed by the following equation:

$$\%\chi_c = \frac{\Delta H_m}{X_{PCL}\Delta H_m^\circ} \times 100$$

where $\%\chi_c$ is the percentage crystallinity, ΔH_m is the apparent enthalpy of fusion per gram of the blends, X_{PCL} is the PCL weight fraction and ΔH_m° is the thermodynamic enthalpy of fusion per gram with an assumed degree of crystallinity of 100% (ΔH_m° = 142 J/g).[27] To obtain an accurate X_{PCL}, the same volumes of PCL solution and ormoglasses involved in the slurries where lyophilized and then weighted (see Table S1 in the Supporting Information).

Fibrous scaffolds were also characterized by thermogravimetric analysis (DSC, Q-600, TA Instruments, New Castle, DE). Samples of approximately 3 mg were placed in alumina crucibles under air atmosphere and heated from 20 °C up to 900 °C at a rate of 10 °C/min.

2.5. Mechanical Tests. Young's modulus, tensile strength, and strain to failure of the fibrous sheets were determined with a Zwick-Roell Zwicki-Line Z0.5TN (Zwick-Roell, Ulm, Germany) universal testing machine, with 10 samples of 40 × 10 mm^2 for each composition. The tensile stress test was monitored at a speed of 10 mm/min.

2.6. pH and Ca^{2+} Release. Continuous pH and Ca^{2+} concentration evaluation of samples at the first stages after aqueous immersion was performed using a Crison GLP22+ pH-meter (Crison Spain), a Crison pH microelectrode, a Crison Ca^{2+} selective electrode, and a Ag/AgCl reference electrode. Measurements were carried out in 1 mL of a 0.02 M KCl and 2.5 mM of $CaCl_2$ saline solution with constant ionic strength and pH ∼ 7.4 ± 0.1. Discrete pH and Ca^{2+} measurements at different time points were collected using the same setup but using 4-(2-hydroxyethyl)-1-piperazineethanesulfonic acid (HEPES) as pH buffer at pH ∼ 7.4 ± 0.1 renewing the liquid at each time point.

2.7. Contact Angle Measurement. The wettability of the surfaces of the samples was evaluated through the water contact angle using the sessile drop method for pure hydrophobic PCL fibers and the captive bubble method for hybrid fibers. The captive bubble method is used to measure highly hydrophilic porous samples that cannot be measured by a conventional sessile one. In this case, material is reversely immersed in ultrapure deionized water and a 3 μL air bubble is generated in the bottom of the water receptacle. The contact angle between solid and liquid is the result of the difference between 180° and the measured bubble angle. Measurements were carried out with a contact angle device coupled with a digital camera (Contact Angle System OCA15plus, Dataphysics, Germany) and analyzed with the SCA20 software (Dataphysics, Germany).

2.8. Atomic Force Microscopy (AFM) Measurements. Fiber stiffness (DMT modulus[28]) and roughness (R_q or RMS) were investigated using AFM (MultiMode 8 atomic force microscope, Bruker and NanoScope Analysis, v1.2, Germany) in PeakForce tapping mode in air after having deposited the thin layer of fibers on an adhesive substrate. Image treatment and data analysis were performed using Gwyddion open-source software for scanning probe microscopy (SPM) data analysis.[29]

2.9. ζ-Potential. The ζ-potential is the electrostatic potential that exists at the surface of the fibers, which is associated with the electric field generated by the atoms in the surface and the local environment of the particle. ζ-potential measurements were carried out using a SurPASS apparatus and VisioLab software (Anton Paar Ltd.). All the measurements were performed at a dynamic pH of the electrolyte (KCl 1 mmol, pH 3−8) using the Adjustable Gap Cell for samples of 10 × 20 mm^2.

2.10. Cell Proliferation Assay. The level of cell proliferation (MC3T3-E1 cells) was measured using a cell counting kit-8 (CCK-8) according to the manufacturer's instructions (Dojindo Molecular Technologies, Inc., Japan). The cells were seeded on each scaffold (10 mm diameter) at a density of 5 × 10^3 cells/specimen previously sterilized with ethylene oxide gas. At each culturing period (1, 3, 5, and 7 days), the culture medium was decanted, and 10 μL of CCK-8 solution was added to each sample and immersed at 37 °C for 3 h. The absorbance at 450 nm was read using a microplate reader (Molecular Devices, Sunnyvale, CA).

2.11. Scanning Electron Microscopy (SEM) for Cell Proliferation. In parallel, same conditions as proliferation assays were applied for samples to be observed by SEM (Hitachi 3000, Japan). Samples were seeded 7 days and then fixed for 10 min at room temperature in 2.5% glutaraldehyde in phosphate buffered saline (PBS). The fixed samples were then dehydrated for 5 min in increasing concentrations of ethanol (75%, 95% and 100%) and critical-point dried. Finally, the samples were coated with a thin layer of gold and examined by SEM under operation at an accelerating voltage 10.0 kV. Images were artificially colored using orange for cell surface and blue for cell filopodia. The use of ImageJ software[26] allowed the evaluation and quantification of the areas occupied by cells and filopodia, together and separated, which are represented as occupied percentage of the total picture area.

2.12. Alkaline Phosphatase Assay. The osteoblastic differentiation of the MC3T3-E1 cells was determined by measuring the ALP activity expressed by the cells on the scaffolds (25 mm diameter) previously sterilized with ethylene oxide gas. The cells were seeded at a density of 1.25 × 10^4 cells on each sample, and cultured in osteogenic α-modified Eagle's medium (α-MEM) supplemented with 10% FBS, 50 μg/mL sodium ascorbate, 10 mM β-glycerol phosphate, and 10 nM dexamethasone for 7, 14, and 21 days. Twenty μg of total protein was added to 50 μL of a *p*-nitrophenyl phosphate solution (Bio-Rad) and incubated for 60 min to assist the enzymatic reaction of ALP on the p-nitrophenyl phosphate substrate. The p-nitrophenol produced by the reaction was measured by the absorbance at 405 nm using the Elisa Plate Reader.

2.13. Western Blotting. Western blot analysis was performed to assess osteogenesis on day 21. Samples (25 mm diameter) previously sterilized with ethylene oxide gas were homogenized in RIPA buffer. Lysates were centrifuged at 12 000 rpm for 10 min at 4 °C. Protein concentrations were determined by the Bradford method. Subsequently, proteins were separated by 10% sodium dodecyl sulfate polyacrylamide gel electrophoresis and transferred electrophoretically to polyvinylidene difluoride membrane. Nonspecific binding was blocked by immersing the membrane in 5% nonfat dry milk for 1h at room temperature. The membrane was then incubated with primary antibodies against osteopontin (OPN) (1:1000; polyclonal, Abcam, Cambridge, MA) and glyceraldehyde 3-phosphate dehydrogenase (GAPDH) (1:1000; polyclonal, Santa Cruz Biotechnology, Santa Cruz, CA) at 4 °C overnight. The membrane was washed and further

incubated with horseradish peroxidase-conjugated antirabbit IgG (1:5000; Santa Cruz Biotechnology, Santa Cruz, CA). The blots were developed using the enhanced chemiluminescence method (Amersham Pharmacia Biotech).

2.14. Quantitative Real-Time Polymerase Chain Reaction (PCR). At the osteogenic period of 7, 14, and 21 days, the expression of the bone-associated genes, including ALP, collagen type I (Col I), osteopontin, and osteocalcin (OCN), was confirmed by quantitative real-time PCR. The first strand cDNA was synthesized from the total RNA (1 μg) using a SuperScript first strand synthesis system for real-time PCR (Invitrogen) according to the manufacturer's instruction. The reaction mixture was made up to 50 μL. Real-time PCR was performed using SYBR GreenER qPCR SuperMix reagents (Invitrogen). The relative transcript quantities were calculated using the $\Delta\Delta$Ct method with GAPDH, as the endogenous reference gene amplified from the samples. The primer sequences of the genes are summarized in Table S2 (see the Supporting Information).

2.15. In Vivo Test for Biocompatibility. Male Sprague−Dawley rats (250−300 g) were used for the study. Animals were housed under standard conditions of temperature (23 ± 1 °C), alternating periods of 12 h in light and dark conditions and fed a standard pellet diet and water ad libitum. The animal experiments were approved by Dankook University Institutional Animal Care and Use Committee, approval number DKU-10-018.

Round shape membranes of 16 mm in diameter were implanted on the backs of rats. Scaffolds were sterilized with ethylene oxide gas before surgical operation. Animals were anesthetized by intramuscular injection with a mixture of Ketamine HCl (80 mg/kg body weight) and Xylazine (10 mg/kg body weight). The back area of rats was shaved and prepared with alcohol and betadine solution. A 2 cm long incision was made on the midportion of the back. Four small pockets were formed subcutaneously with baby metzenbaum scissors on the backside in a lateral direction from the spine of each rat, and the membranes were inserted. Each animal received one type of scaffold composition (PCL, PCL-S40, or PCL-S52 membranes). The incision was subsequently closed with 4-0 nonabsorbable monofilament suture material (Prolene). Animals were euthanized, and implanted membranes were extirpated at 4 weeks for histologic analysis. Four samples per membrane were used for the in vivo biocompatibility study. Tissues surrounding the implanted films were placed in 4% buffered formaldehyde for 24 h at room temperature, dehydrated serially in a graded ethanol, paraffin embedded, sectioned, and stained with hematoxylin and eosin (HE) or Masson's trichrome (MT) stain. Samples were examined with light microscopy for the biocompatibility study. Histological score was done from both stained slides. The scoring includes the extent of inflammatory response, thickness of fibrous capsule, presence of blood vessels, and proliferation of fibroblasts (from absence to severe, score 0 to 3, Table S3 in the Supporting Information). Tissue sections were immunostained for vWF, a protein present in blood vessel basement membranes, and imaged by light microscope. In order to determine the quantity of the newly formed blood vessels, indicated by vWF staining, we counted the number of vessels manually at 200× magnification in the membrane, and normalized to membrane area with the use of Scion Image Software (Scion Corporation, Frederick, MD).

2.16. Statistical Analysis. Results are shown as the mean ± standard deviation and analyzed via one-way ANOVA. A value of $p < 0.05$ was considered statistically significant (*) and $p < 0.001$ highly statistically significant (**).

3. RESULTS AND DISCUSSION

3.1. Morphological Characterization and Mechanical Evaluation. The production of different blends of ormoglass/PCL with different Si contents (and thus different calcium contents) was successful. FE-SEM images of the three different Si content samples can be observed in Figure 1. No segregation of inorganic phases was observed even at higher magnifications, suggesting a good homogeneity between the ormoglass and the polymeric PCL matrix. However, few beads were present,

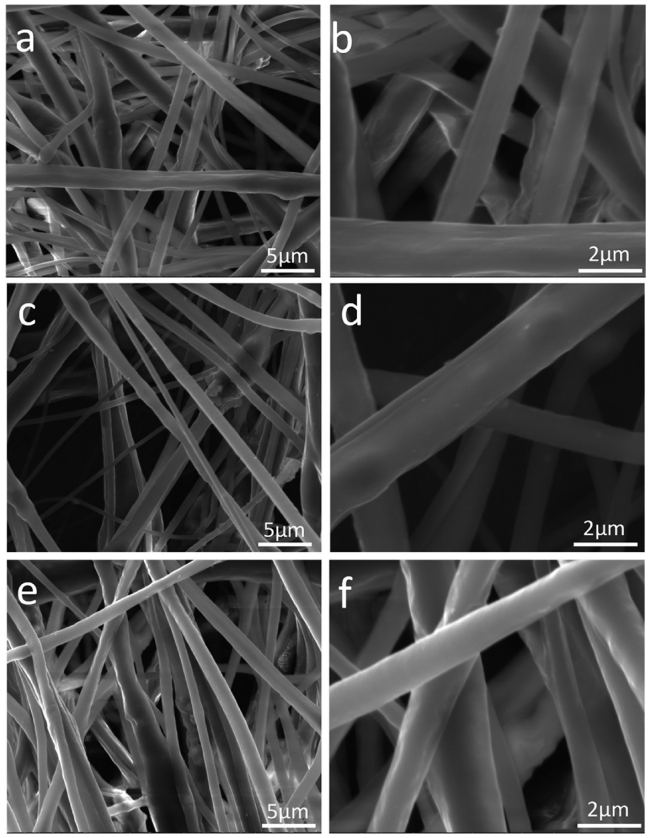

Figure 1. FE-SEM images of hybrid nanostructured fibers of (a,b) PCL-S40, (c,d) PCL-S52, and (e,f) PCL-S70.

indicating that further efforts should be made to improve the relation between solvent vapor pressure and distance from the tip to the collector. Fiber thicknesses (Table 1) did not significantly change among the fibers, being around 2 μm. EDS allowed the quantification of the composition of fibers, which was close to nominal composition (Table 1).

Tensile-strain assays showed that the more Si content, the higher the Young's modulus. However, a maximum in tensile strength was found for PCL-S52. It also had the highest strain to rupture of the blends. Results seem to confirm that the content of Si directly influences the strength of the gelated network, which acts as a reinforcement. Mechanical resistance drops when Si content is decreased.

3.2. Thermal Characterization. Thermogravimetric analysis revealed that the inorganic content increase with the decrease of Si content, probably due to the higher molecular weight of, especially, P_2O_5 in front SiO_2 (see Table S1 in the Supporting Information). DSC analysis showed a melting peak at ∼56 °C and a decomposition peak at ∼400 °C for all the samples. However, a small shift was observed as the Si content was modified (see Table S1 in the Supporting Information). Degree of crystallinity ($\%\chi_c$) was also assessed. PCL-S40 had the most crystalline structure (35.9%), similar to that of pure PCL (35.8%). In the rest of the blends, the $\%\chi_c$ slightly decreased with the increase of the Si content (34.5 and 33.3% for PCL-S52 and PCL-S40, respectively).

3.3. Surface Evaluation. Water contact angle measurements were performed, and gradual hydrophilicity augmentation was observed as Si content was increased (Table 1). Water contact angles of all hybrid samples dramatically dropped compared with pure PCL (130.3 ± 0.8°) measured by sessile

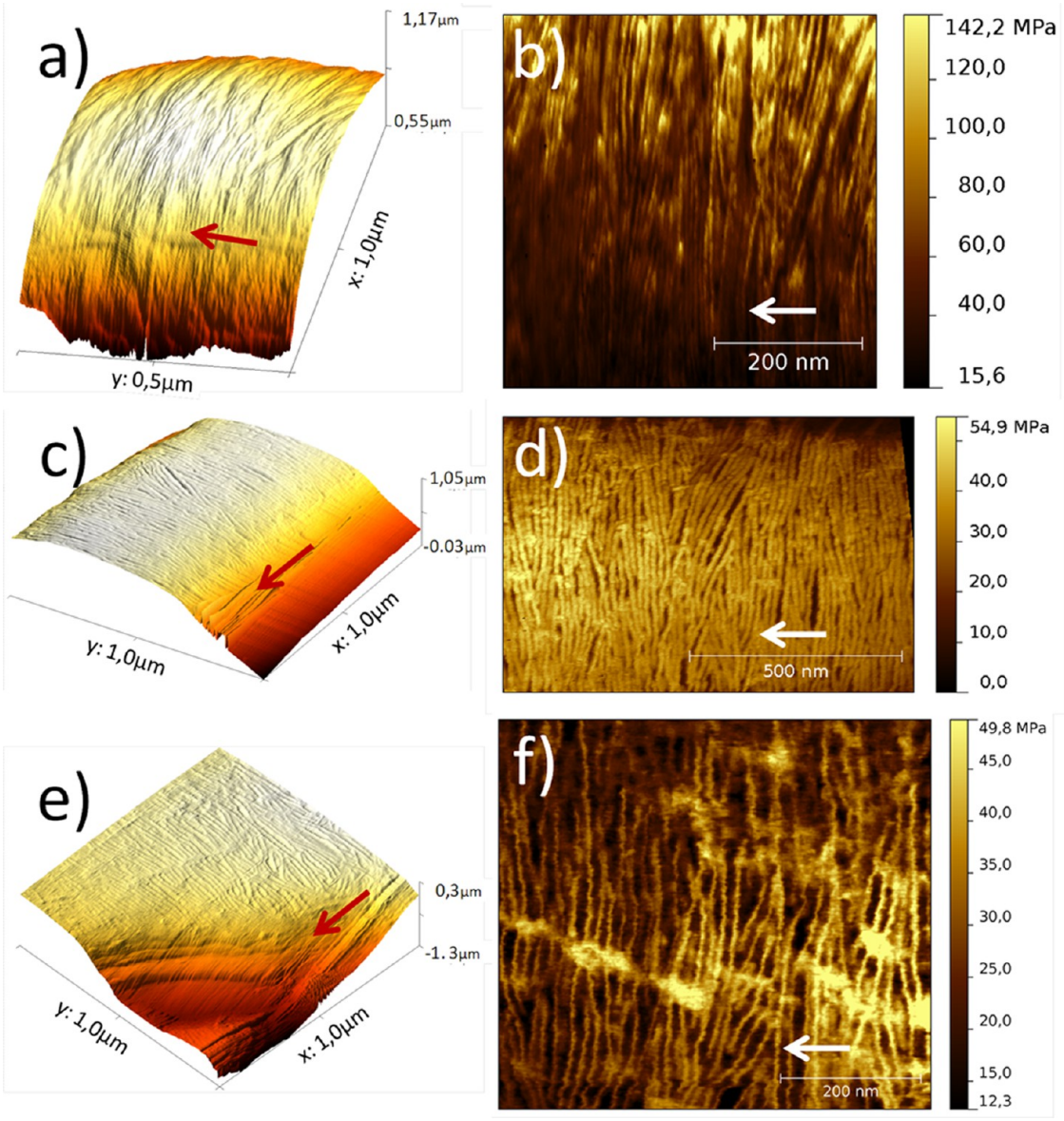

Figure 2. Three-dimensional plots of AFM topographic images and DMT modulus maps for (a,b) PCL-S40; (c,d) PCL-S52, and (e,f) PCL-S70. Arrows show the direction of the fibers.

drop method. it can be inferred that the hydrophilic character of calcium and phosphorus compounds highly influences surface properties compared to pure PCL fibers, and an improvement of the cell adhesion could be expected according to a previous work performed by our group.[30] There, Charles-Harris et al. suggested that osteoblast-like MG63 cells prefer to adhere directly to hydrophilic calcium phosphate glasses instead of polylactic acid (PLA), which had similar hydrophobicity than PCL.[31] Also Serra et al.[32] observed that scaffolds formed by a dispersion of calcium phosphate glass microparticles in a PLA/PEG blend improved rat mesenchymal stem cells (rMSC) spreading.

AFM measurements showed relevant differences among the fibrous scaffolds. The presence of spherulites, whose lamella folds were perpendicularly oriented to the direction of the fiber, indicated a clear anisotropic distribution. Stiffness (DMT modulus) and roughness (RMS) measured by AFM are also presented in Table 1. In general, DMT values of the hybrid fibers are much lower than what pure PCL fibers can offer.[33] There is a clear influence of the Si content within the fibers as the lower the Si content, the higher the stiffness, in contrast with tensile-strain assays. We have to take into account that DMT modulus can only obtain information on the first few nanometers of the surface. Roughness showed a slightly increasing tendency toward higher contents of silicon due to the increase of the lamella periods (see Scheme S2 in the Supporting Information). This phenomenon can be explained by a possible lower compression resistance of the ormoglass with less silicon, which is compacted like a sandwich. Rough 3D images and DMT modulus maps are shown in Figure 2. The decrease of the RMS with the decrease in Si content can be associated with a lower separation between lamellas, which can induce a further densification of the material. This phenomenon suggests that a possible increase of the crystallinity within the blends has occurred yielding a correlated increase of stiffness. This fact can also be observed in other polymers such as PLA[34] and was also confirmed by DSC $\%\chi_c$ calculations, which showed that the lower the Si content, the higher the $\%\chi_c$.

dx.doi.org/10.1021/am500885v | ACS Appl. Mater. Interfaces 2014, 6, 7512−7522

However, they were lower than pure PCL $\%\chi_c$ excepting PCL-S40 one. Then, differences between the three hybrid samples can only be due to the different composition. Thus, the higher the Si content, the lower the stiffness. This result suggests that there is an intimate interaction between the hybrid and the polymer, which can greatly affect the stiffness of the material and, therefore, the cell response.[35] We can also infer that the stiffness of the material can be easily modulated by a change in the composition.

Different ζ-potentials were observed. ζ-potential versus pH plots (Figure 3) showed a significant increase of the surface

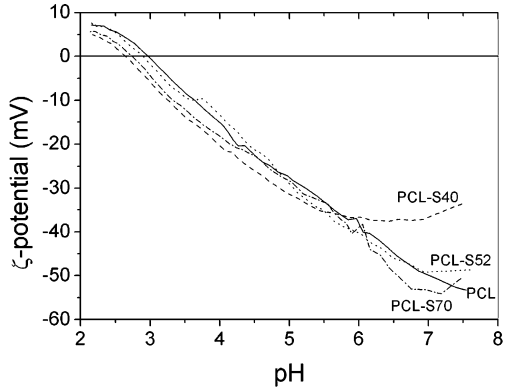

Figure 3. ζ-potential/pH plot of the three different compositions compared with pristine PCL fibers (solid), PCL-S70 (dash-dots), PCL-S52 (dots), and PCL-S40 (dashes).

charge for PCL-S40 compared with the rest of the fibrous scaffolds. PCL has the most negative value (−52.7 mV) at physiological pH, that may be explained by the preferential orientation of carbonyl groups at the surface.[36] PCL-S70 and PCL-S52 have slightly more positive potentials (−51.4 and −48.7 mV, respectively). Surprisingly, PCL-S40 has a significant more positive value (−34.4 mV). pH at the isoelectric point (ζ-potential = 0) has similar tendency. Meanwhile, the isoelectric points are located at pH = 3.0, 2.7, and 2.9 for PCL, PCL-S70, and PCL-S52, respectively; the isoelectric point for PCL-S40 is located at pH = 2.6, which was the lowest one surprisingly. It presented the most positive surface charge even though it is still negative at physiological pH. A recent study showed that cells, in this case fibroblasts, have a better affinity for positively charged matrices[37] for adhesion. This aspect could explain the better adhesion behavior[38−40] of PCL-S40 and, thus, an enhanced further differentiation.

3.4. Ion Release and pH Measurements. The lower the Si content, the higher the calcium release. Calcium release and pH were measured in almost pristine conditions at pH ∼ 7.4 in order to obtain a narrow approach of the phenomena happening at the material interface. For this reason, absence of buffer solution was applied as a method to reveal the effect of the material on the surrounding fluid, especially on the immediate interface. The initial solution also contained Ca^{2+}, similar to the c-SBF solution developed by Oyane et al.,[41] in order to have enough calcium ions in case the material adsorbs it (Figure 4a). In all cases, pH reached values comprised between 9.4 and 9.5, what is correlated with the release of Ca^{2+}, whose higher release is associated with the lower content of silicon in the sample. Peaks and valleys were observed. They can be associated with the dynamic equilibrium adsorption−

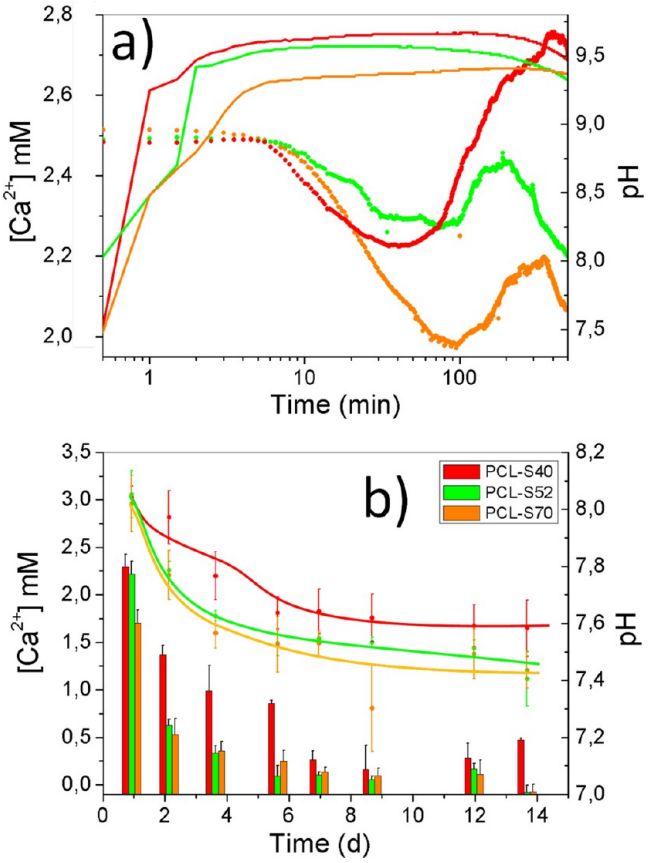

Figure 4. (a) pH and Ca^{2+} release in continuous. For pH curves (continuous line), right axis should be considered, meanwhile for Ca^{2+} concentration (dense circles) the left one should be considered. Notice that the *x*-axis is in logarithmic scale. (b) Monitorized pH and Ca^{2+} at different time points. For pH measurements (dense circles), right axis should be considered, meanwhile for Ca^{2+} concentration (columns) the left one should be considered.

desorption of calcium ions on the surface, which seems to be desorption-favored due to the weak chelating capacity of the surface of the material. Calcium release and pH discrete measurements at longer time points, using HEPES as buffer at pH ∼ 7.4, were also analyzed and are presented in Figure 4b. PCL-S40 is the sample that maintains a higher and sustained release of Ca^{2+} with time. PCL-S52 has a similar initial burst of Ca^{2+}, reaching more than 2 mM of Ca^{2+} the first day, but dropping faster afterward. PCL-S70, as expected, was the sample with the lowest Ca^{2+} release. In agreement with Figure 4a, the higher the Ca^{2+} release, the higher the pH, which tends to be stabilized at pH ∼ 7.4 at longer times when the Ca^{2+} release decreases. These results suggest that the Si content decrease in fiber composition (linked to an increase of the Ca^{2+} and P^{5+} of the composition) led to an increase in the release of Ca^{2+} in the form of $Ca(OH)_2$, which is responsible for the increase of the pH up to around 9.5. P^{5+} in the form of $H_{3-x}PO_4^{x-}$ seems to be responsible for the slightly acid compensation until reaching a constant pH around 9. No significant differences were found among the three samples in pH at early stages of the immersion. Accordingly, at early stages and longer times Ca^{2+} release measured by a selective electrode was higher as the content of silicon decreased. PCL-S40 was the sample with a higher release rate of calcium and the most constant sustained decrease at higher time points. At longer

dx.doi.org/10.1021/am500885v | ACS Appl. Mater. Interfaces 2014, 6, 7512−7522

time points, there is still ormoglass protected by the PCL that is released only when PCL is degraded. For the case of PCL-S52 and PCL-S70, the remained calcium is lower as its initial content was also lower than that of PCL-S40, which continued being the composition with the highest calcium and most sustained release.

3.5. In Vitro Evaluation. PCL-S40 showed the best cell-material interaction. Typical SEM pictures of previously fixed MC3T3-E1 cells are presented in Figure 5a–d for the different

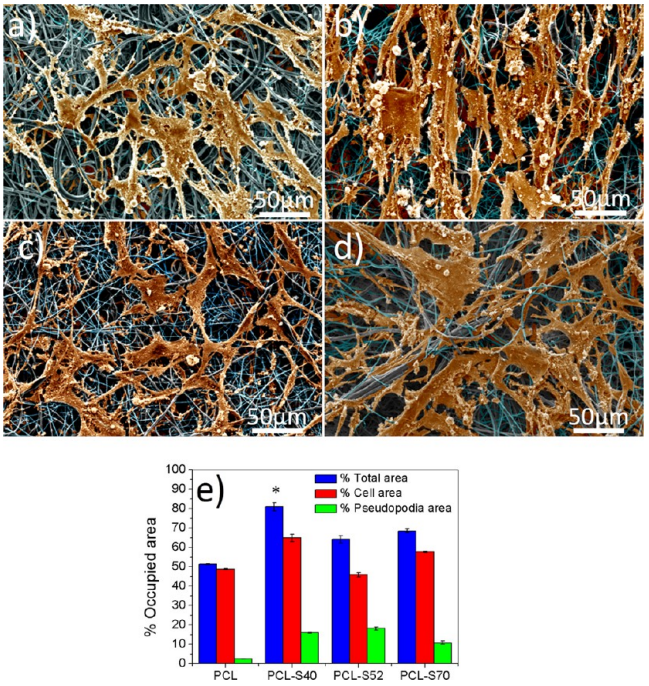

Figure 5. Cell adhesion images on the fibrous scaffolds. In (a–d), cells and filopodia were artificially colored in order to calculate surface occupation in (e).

samples. Cells and filopodia were artificially colored ,and the surface measured (Figure 5d). The relative surface occupied by cells in sample PCL-S40 is significantly higher than the rest. However, the surface occupied by filopodia is similar for the three hybridized samples (Figure 5e). Also, results of proliferation tests are plotted in Figure 6a. The proliferation was improved for all hybrid fiber compositions in comparison to PCL fibers that were used as control. PCL-S40 fibers especially induced the best proliferation at 7 days of culture. Both results confirm the best cell-material interaction for PCL-S40.

PCL-S40 enhanced MC3T3-E1 cells differentiation over the rest of the samples. Results on ALP activity showed an increase for all compositions at day 14 and a decrease at day 21 (Figure 6b). The level of alkaline phosphatase (ALP) activity of PCL-S40 samples at 14 days is enhanced, whose difference is highly statistically significant. Related to OPN, similar results to ALP were observed by Western blot (Figure 6c and d). PCL-S40 samples trigger the expression of a significant higher amount of protein than the other compositions. In fact, it has the higher OPN/GAPDH ratio. Quantitative real-time-PCR of the expression of the different bone-associated genes, including ALP, is shown in Figure 7. PCL-S40 is the sample that shows the most marked gene expression in all the markers. As expected, early markers such as COL 1 and ALP showed the

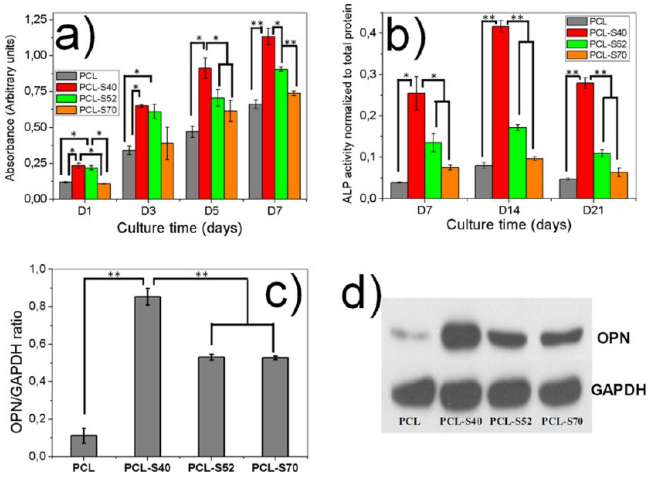

Figure 6. (a) Cell proliferation on fibers with different Si contents at different time points. (b) ALP activity expressed by the cells on the scaffolds. (c) ONP/GAPDH ratio for different Si contents. (d) Western blot results enhanced with a chemiluminescence method.

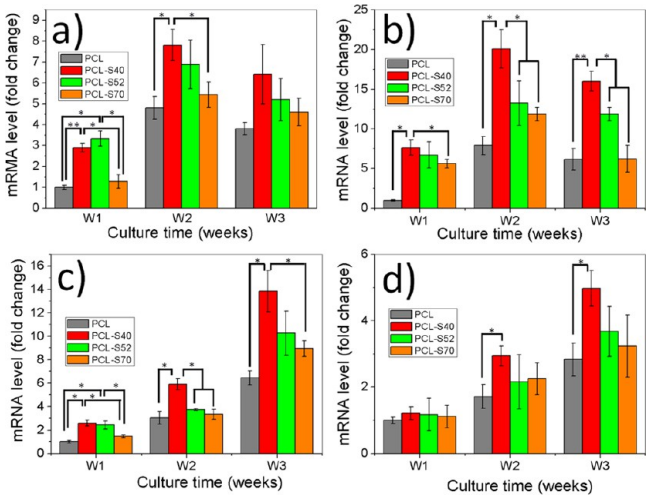

Figure 7. Expression of the bone-associated genes confirmed by quantitative real-time PCR for (a) collagen type I (Col I), (b) ALP, (c) osteopontin (OPN), and (d) osteocalcin (OCN).

highest levels of expression in the 2 weeks' time point of cell culture, correlating with the early stages of cell differentiation. Meanwhile, OPN and OCN, later markers of bonelike cell differentiation, showed a maximum expression after 3 weeks of cell culture, corresponding with early stages of mineralization. Thus, from the results reported in this work, PCL-S40 shows the highest levels of Ca^{2+} release that has been demonstrated to have an effect on the enhancement of the expression of bone related proteins such as ALP, Col 1, OPN, OC, and mineralization.[42]

3.6. In Vivo Evaluation. Miron and Zhang defined an osteoinductive material as the one that should be capable of inducing ectopic bone formation when implanted into extraskeletal locations; in other words, it should be osteogenic in soft tissues.[43] Therefore, the tissue response to the three membrane compositions implanted subcutaneously in dorsal region of rats was evaluated, and each animal received four scaffolds. The recovery from the anesthesia was uneventful. After implantation, all animals showed normal healing process without inflammation and remained in good health during the

study period. The incision sites healed normally and no inflammatory signs and material related complications were observed. The membranes used in this study resulted in satisfactory healing. The membranes of the PCL polymeric biomaterials were explanted at 4 weeks after implantation along with the tissues surrounding the implant. At harvesting, the samples and surrounding tissues showed no macroscopically redness or inflammation. Nanofibrous PCL membrane was utilized as control for assessment of inflammatory tissue responses. Analyses of the responses by microscopic histological observation are summarized in Table S3 (Supporting Information).

Numerous vessels were observed overall area of the mats. Micrographs of the rat subcutaneous tissue response to the pure PCL membrane are shown in Figure 8a and b. No

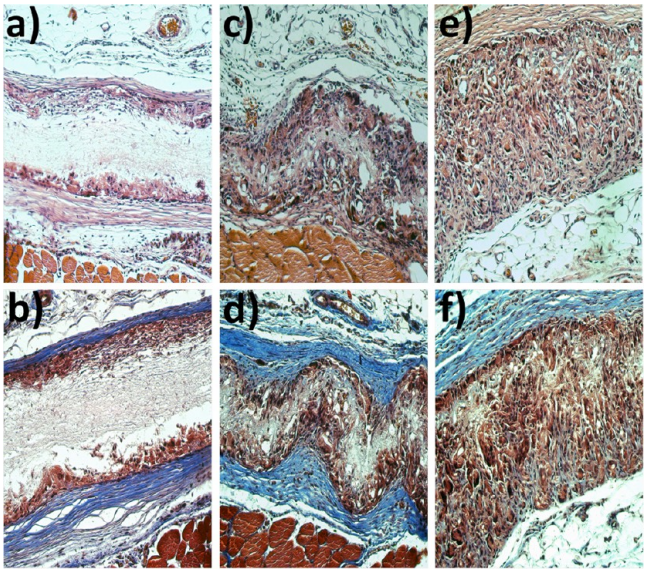

Figure 8. Microscopic images of rat subcutaneous tissue response to the (a,b) PCL membrane, (c,d) PCL-S40, and (e,f) PCL-S52 (HE stain: a, c, e; MT stain: b, d, f; original magnification ×200).

significant immune response was detected and fibrous capsule surrounded PCL membrane. Fibroblasts arranged around the membrane and approximately 15−20% of the membrane was changed to fibrous tissue with fibroblast infiltration. Few vessels were also observed within infiltrated fibrous tissue and the surrounding area. Biocompatibility responses to PCL-S40 membranes are described in Figure 8c and d. The overall characteristics of this membrane were similar to PCL membrane. The membranes evoked a minimum immune response after 4 weeks of subcutaneous implantation. Fibrous capsule formation around the membrane is evident and approximately 50% of the membrane was changed to fibrous tissue with fibroblast and vessel infiltration. Representative photographs of PCL-S52 membrane and surrounding tissue are shown in Figure 8e and f. The observations are nearly the same with minimum infiltration of inflammatory cells and good biocompatibility compared with PCL and PCL-S40 membrane. Inflammatory cells were discovered only on few parts of surrounding fibrous capsule. Fibrous tissue infiltration into the membrane was more prominent than other two membranes and approximately 85% of the membrane was changed to fibrous tissue with fibroblasts. Surprisingly, abundant vessels were observed over the entire area of the membrane.

PCL-S40 showed the highest number of new blood vessels. To quantify enhanced blood vessel formation within membrane area, immunohistochemical staining of the blood vessel endothelial specific marker vWF was used (Figure 9a−c).

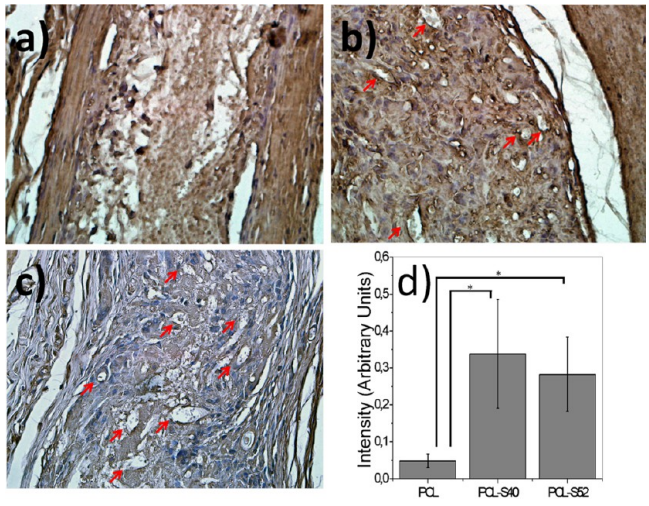

Figure 9. Staining optic microscopy images for vWF of the fibrous membrane scaffolds at 4 weeks, ×400 magnification: (a) PCL, (b) PCL-S40, and (c) PCL-S52. Red arrows denote newly formed vessels within the membrane area. (d) Quantification of the immunohistochemical staining of vWF of vessels in each study group, ×200.

Significant differences were observed for blood vessel formation on immunostaining slides reading results for analyzing vWF expression. PCL-S40 (0.338 ± 0.147) and PCL-S52 (0.282 ± 0.1) groups demonstrated more prominent angiogenesis ratio than PCL (0.048 ± 0.017) group (Figure 9d). PCL-S40 and PCL-S52 groups showed similar results of angiogenesis and did not show significant difference. The newly formed blood vessels were distributed homogeneously into the membrane in all conditions. PCL-S40 (p = 0.004) and PCL-S52 (p = 0.003) groups revealed significantly increased number of new blood vessels than in PCL group (Figure 9d).

Biological results not only confirm the osteogenic potential of the composition with less Si content, but also suggest a better angiogenic effect. The higher and sustained release of free calcium to the media seems to play a key role in the promotion of blood vessel formation, as in vivo results show, as corroborates other results with high biodegradable glasses that has an important release of Ca^{2+} due to fast degradation.[44] These results seem to match with hypothesis described in the works of Aguirre and co-workers:[7,45] calcium ions seem to have a crucial role in angiogenesis process due to the existence of CaSR. Considering that angiogenesis is the process that allows the formation of blood vessels from preexisting ones, almost all regenerative scaffolds in tissue engineering require the creation and colonization of blood vessels for the correct cell migration, signaling, oxygen and nutrients diffusion and residues elimination.[46] It is also known that scaffolds can trigger angiogenesis through mechanical and biochemical signaling synergistic pathways. The biochemical signaling is controlled by the calcium-sensing receptor (CaSR),[7] a trans-membrane protein receptor able to detect and discriminate extracellular calcium concentration in media and at the materials interface. Both signals trigger a synergistic effect by the activation of endothelial progenitor cells (EPCs)-mediated vascular endo-

dx.doi.org/10.1021/am500885v | ACS Appl. Mater. Interfaces 2014, 6, 7512−7522

thelial growth factor (VEGF) and VEGF receptor 2 (VEGFR-2) expression, which promote progenitor cell homing, differentiation and tubulogenesis. Eventually, when Ca^{2+} concentration reaches a determined level, CaSR initiates a biased biochemical cascade, which leads to the production of VEGF, crucial for tube formation and vascularization of tissues. MC3T3 cells have been demonstrated to present this receptor. Moreover, extracellular calcium has been shown to promote their chemotaxis and proliferation.[47] Accordingly, the sample with a higher promotion of the production of VEGF, as can be inferred by observing in vivo results, had the highest number of blood vessels (Figure 9).

On the other hand, the mechanosensitive signaling is upregulated by nonmuscle myosin II contraction. Thus, the effect of the stiffness in the angiogenic promotion of these materials should be further studied, eliminating the variable of the calcium release, as it is well-known that stiffness can promote angiogenesis.[48] But reported evidence of angiogenic stiffness promotion involve ranges around the KPa order of magnitude, far from the range shown in this study (~MPa), in contrast with the case of bone, which can reach ~GPa.[49]

Further in vitro studies should be performed focusing on the potential angiogenic effect of these materials using, for example, chicken embryo chorioallantoic membrane (CAM) assay or network formation with human umbilical vein endothelial cells (HUVECs) or human endothelial progenitor cells (hEPCs).

Finally, this work has been developed using the electrospinning deposition method for the fabrication of nanostructured fibers. However, this blended material can be adapted for other scaffold production methods, depending on the application (rapid prototyping, solvent casting/particle leaching, as filler, etc.). This material blend has emerged as a promising and versatile candidate for biomedical applications and models that require the infiltration and colonization of a blood vessel network.

4. CONCLUSIONS

A new family of bioactive nanostructured fibers was produced by electrospinning. The materials developed are based on a hybrid organic/inorganic blend comprising by an organometallic network and a biodegradable polymer. The obtained fibers showed an homogeneous structure, a rough surface, and mechanical instability, as well as excellent osteogenic features. Results suggest that modification of the ormoglass composition modulates the release of Ca^{2+} in the proper rate to activate VEGF production cascade thanks to CaSR. This seems to support the hypothesis, which considers the Ca^{2+} released by the fibers of PCL-S40 as crucial for its higher degree of angiogenesis. In vivo results also seem to support this thesis.

■ ASSOCIATED CONTENT

Supporting Information

Authors offer some data essential to the specialized reader. Schemes, figures, and tables that contribute to further detail this paper. This material is available free of charge via the Internet at http://pubs.acs.org.

■ AUTHOR INFORMATION

Corresponding Author

*Mailing address: Institute for Bioengineering of Catalonia. C/ Baldiri I Reixac, 15-21. 08028 Barcelona (SPAIN). Tel: +34934020211. Fax: +34934020183. E-mail: ocastano@ibecbarcelona.eu.

Author Contributions

O.C. and H.-W.K. conceived and designed the experiments; O.C., N.S., E.X., J0-H.P., G.-Z.J., T.-H.K., and J.-H.K. performed the experiments; O.C., N.S., E.E., G.-Z.J., T.-H.K., and J.-H.K. analyzed the data; O.C., H.-W.K., and J.A.P. contributed reagents/materials/analysis tools. O.C. wrote the manuscript.

Notes

The authors declare no competing financial interest.

■ ACKNOWLEDGMENTS

We thank the European Commission (European ERANET project PI11/03030, NANGIOFRAC) and the Spanish Ministry of Economy and Competitiveness (Project MAT2011-29778-C02-01) for funding. O.C. also acknowledges the MINECO for the "Ramon y Cajal" contract and the "José Castillejo" mobility allowance. This work was also partially supported by a grant from Priority Research Centers Program (2009-0093829), National Research Foundation of Korea.

■ ABBREVIATIONS

AFM, atomic force microscopy
ALP, alkaline phosphatase
CaSR, calcium sensing receptor
cDNA, cDNA
Col I, collagen type I
DMT, Derjaguin−Muller−Toporov based model
EDS, energy dispersive spectrometry
FESEM, field emission scanning electron microscopy
GAPDH, glyceraldehyde 3-phosphate dehydrogenase
HEPES, 4-(2-hydroxyethyl)-1-piperazineethanesulfonic acid
MC3T3-E1 cells, osteoblast precursor cell line derived mouse calvaria
OCN, osteocalcin
OPN, osteopontin
ORMOGLASS, organically modified glass
PCL, polycaprolactone
PCR, polymerase chain reaction
Rq or RMS, root mean squared
rMSC, rat mesenchymal stem cells
RNA, ribonucleic acid
SPM, scanning probe microscopy
TEOS, tetraethylorthosilicate
VEGF, endothelial growth factor
VEGFR-2, vascular endothelial growth factor receptor 2
vWF, von Willebrand factor

■ REFERENCES

(1) Brown, E. M.; MacLeod, R. J. Extracellular Calcium Sensing and Extracellular Calcium Signaling. *Physiol. Rev.* **2001**, *81* (1), 239−297.

(2) Mentaverri, R.; Yano, S.; Chattopadhyay, N.; Petit, L.; Kifor, O.; Kamel, S.; Terwilliger, E. F.; Brazier, M.; Brown, E. M. The Calcium Sensing Receptor Is Directly Involved in Both Osteoclast Differentiation and Apoptosis. *FASEB J.* **2006**, *20* (14), 2562−2564.

(3) Adams, G. B.; Chabner, K. T.; Alley, I. R.; Olson, D. P.; Szczepiorkowski, Z. M.; Poznansky, M. C.; Kos, C. H.; Pollak, M. R.; Brown, E. M.; Scadden, D. T. Stem Cell Engraftment at the Endosteal Niche Is Specified by the Calcium-Sensing Receptor. *Nature* **2006**, *439* (7076), 599−603.

(4) Tommila, M.; Jokilammi, A.; Terho, P.; Wilson, T.; Penttinen, R.; Ekholm, E. Hydroxyapatite Coating of Cellulose Sponges Attracts Bone-Marrow-Derived Stem Cells in Rat Subcutaneous Tissue. *J. R. Soc. Interface* **2009**, *6* (39), 873−880.

(5) Yamauchi, M.; Yamaguchi, T.; Kaji, H.; Sugimoto, T.; Chihara, K. Involvement of Calcium-Sensing Receptor in Osteoblastic Differentiation of Mouse MC3T3-E1 Cells. *Am. J. Physiol.: Endocrinol. Metab.* **2005**, *288* (3), E608−E616.
(6) Hoeben, A.; Landuyt, B.; Highley, M. S.; Wildiers, H.; Van Oosterom, A. T.; De Bruijn, E. A. Vascular Endothelial Growth Factor and Angiogenesis. *Pharmacol. Rev.* **2004**, *56* (4), 549−580.
(7) Aguirre, A.; Gonzalez, A.; Navarro, M.; Castano, O.; Planell, J. A.; Engel, E. Control of Microenvironmental Cues with a Smart Biomaterial Composite Promotes Endothelial Progenitor Cell Angiogenesis. *Eur. Cells Mater.* **2012**, *24*, 90−106.
(8) Rezwan, K.; Chen, Q. Z.; Blaker, J. J.; Boccaccini, A. R. Biodegradable and Bioactive Porous Polymer/Inorganic Composite Scaffolds for Bone Tissue Engineering. *Biomaterials* **2006**, *27* (18), 3413−3431.
(9) Engel, E.; Michiardi, A.; Navarro, M.; Lacroix, D.; Planell, J. A. Nanotechnology in Regenerative Medicine: the Materials Side. *Trends Biotechnol.* **2008**, *26* (1), 39−47.
(10) Zhang, X.; Cai, Q.; Liu, H.; Zhang, S.; Wei, Y.; Yang, X.; Lin, Y.; Yang, Z.; Deng, X. Calcium Ion Release and Osteoblastic Behavior of Gelatin/β-Tricalcium Phosphate Composite Nanofibers Fabricated by Electrospinning. *Mater. Lett.* **2012**, *73* (0), 172−175.
(11) Zou, B.; Liu, Y.; Luo, X.; Chen, F.; Guo, X.; Li, X. Electrospun Fibrous Scaffolds with Continuous Gradations in Mineral Contents and Biological Cues for Manipulating Cellular Behaviors. *Acta Biomater.* **2012**, *8* (4), 1576−1585.
(12) Datta, P.; Chatterjee, J.; Dhara, S., Electrospun Nanofibers of a Phosphorylated Polymer-A Bioinspired Approach for Bone Graft Applications. *Colloids Surf., B* **2012**, (0).
(13) Xie, J.; Blough, E. R.; Wang, C.-H. Submicron Bioactive Glass Tubes for Bone Tissue Engineering. *Acta Biomater.* **2012**, *8* (2), 811−819.
(14) Hench, L. L. The story of Bioglass. *J. Mater. Sci.: Mater. Med.* **2006**, *17* (11), 967−978.
(15) Rahaman, M. N.; Day, D. E.; Sonny Bal, B.; Fu, Q.; Jung, S. B.; Bonewald, L. F.; Tomsia, A. P. Bioactive Glass in Tissue Engineering. *Acta Biomater.* **2011**, *7* (6), 2355−2373.
(16) Navarro, M.; Ginebra, M.-P.; Clément, J.; Salvador, M.; Gloria, A.; Planell, J. A. Physicochemical Degradation of Titania-Stabilized Soluble Phosphate Glasses for Medical Applications. *J. Am. Ceram. Soc.* **2003**, *86* (8), 1345−1352.
(17) Eldesoqi, K.; Seebach, C.; Nguyen Ngoc, C.; Meier, S.; Nau, C.; Schaible, A.; Marzi, I.; Henrich, D. High Calcium Bioglass Enhances Differentiation and Survival of Endothelial Progenitor Cells, Inducing Early Vascularization in Critical Size Bone Defects. *PLoS One* **2013**, *8* (11), e79058.
(18) Niemelä, T.; Niiranen, H.; Kellomäki, M.; Törmälä, P. Self-Reinforced Composites of Bioabsorbable Polymer and Bioactive Glass with Different Bioactive Glass Contents. Part I: Initial Mechanical Properties and Bioactivity. *Acta Biomater.* **2005**, *1* (2), 235−242.
(19) Blaker, J. J.; Maquet, V.; Jerome, R.; Boccaccini, A. R.; Nazhat, S. N. Mechanical properties of highly porous PDLLA/Bioglass composite foams as scaffolds for bone tissue engineering. *Acta Biomater.* **2005**, *1* (6), 643−652.
(20) Gonzalez, B.; Colilla, M.; de Laorden, C. L.; Vallet-Regi, M.; Novel, A. Synthetic Strategy for Covalently Bonding Dendrimers to Ordered Mesoporous Silica: Potential Drug Delivery Applications. *J. Mater. Chem.* **2009**, *19* (47), 9012−9024.
(21) Kim, H.-W.; Lee, H.-H.; Knowles, J. C. Electrospinning Biomedical Nanocomposite Fibers of Hydroxyapatite/Poly(Lactic Acid) for Bone Regeneration. *J. Biomed. Mater. Res., Part A* **2006**, *79A* (3), 643−649.
(22) Sachot, N.; Castaño, O.; Mateos-Timoneda, M. A.; Engel, E.; Planell, J. A. Hierarchically Engineered Fibrous Scaffolds for Bone Regeneration. *J. R. Soc. Interface* **2013**, *10* (88), 20130684.
(23) Song, J.-H.; Yoon, B.-H.; Kim, H.-E.; Kim, H.-W. Bioactive and Degradable Hybridized Nanofibers of Gelatin−Siloxane for Bone Regeneration. *J. Biomed. Mater. Res., Part A* **2008**, *84A* (4), 875−884.
(24) Jang, J. H.; Castano, O.; Kim, H. W. Electrospun materials as potential platforms for bone tissue engineering. *Adv. Drug Delivery Rev.* **2009**, *61* (12), 1065−1083.
(25) Kim, H. W.; Kim, H. E.; Knowles, J. C. Production and Potential of Bioactive Glass Nanofibers as a Next-Generation Biomaterial. *Adv. Funct. Mater.* **2006**, *16* (12), 1529−1535.
(26) Rasband, W. S. *ImageJ*; U.S. National Institutes of Health: Bethesda, MD, 1997−2011.
(27) Elzein, T.; Nasser-Eddine, M.; Delaite, C.; Bistac, S.; Dumas, P. FTIR Study of Polycaprolactone Chain Organization at Interfaces. *J. Colloid Interface Sci.* **2004**, *273* (2), 381−387.
(28) Dejarguin, B. V.; Muller, V. M.; Toporov, Y. P. Effect of the Contact Deformations on the Adhesion of Particles. *J. Colloid Interface Sci.* **1975**, *53* (2), 314−326.
(29) Nečas, D.; Klapetek, P. Gwyddion: an Open-Source Software for SPM Data Analysis. *Cent. Eur. J. Phys.* **2012**, *10* (1), 181−188.
(30) Charles-Harris, M.; Koch, M. A.; Navarro, M.; Lacroix, D.; Engel, E.; Planell, J. A.; PLA/calcium, A. phosphate degradable composite material for bone tissue engineering: an in vitro study. *J. Mater. Sci.: Mater. Med.* **2008**, *19* (4), 1503−1513.
(31) Biresaw, G.; Carriere, C. J. Correlation Between Mechanical Adhesion and Interfacial Properties of Starch/Biodegradable Polyester Blends. *J. Polym. Sci., Part B: Polym. Phys.* **2001**, *39* (9), 920−930.
(32) Serra, T.; Planell, J. A.; Navarro, M. High-Resolution PLA-Based Composite Scaffolds Via 3-D Printing Technology. *Acta Biomater.* **2013**, *9* (3), 5521−5530.
(33) Hartman, O.; Zhang, C.; Adams, E. L.; Farach-Carson, M. C.; Petrelli, N. J.; Chase, B. D.; Rabolt, J. F. Biofunctionalization of Electrospun PCL-Based Scaffolds With Perlecan Domain IV Peptide to Create a 3-D Pharmacokinetic Cancer Model. *Biomaterials* **2010**, *31* (21), 5700−5718.
(34) Álvarez, Z.; Mateos-Timoneda, M. A.; Hyroššová, P.; Castaño, O.; Planell, J. A.; Perales, J.; Engel, E.; Alcántara, S. The Effect of the Composition of PLA Films and Lactate Release on Glial and Neuronal Maturation and the Maintenance of the Neuronal Progenitor Niche. *Biomaterials* **2013**, *34* (9), 2221−2233.
(35) Engler, A. J.; Sen, S.; Sweeney, H. L.; Discher, D. E. Matrix Elasticity Directs Stem Cell Lineage Specification. *Cell* **2006**, *126* (4), 677−689.
(36) Vaquette, C.; Babak, V. G.; Baros, F.; Boulanouar, O.; Dumas, D.; Fievet, P.; Kildeeva, N. R.; Maincent, P.; Wang, X. Zeta-Potential and Morphology of Electrospun Nano- and Microfibers from Biopolymers and their Blends Used as Scaffolds in Tissue Engineering. *Mendeleev Commun.* **2008**, *18* (1), 38−41.
(37) Kim, J.-h.; Kim, D.-H.; Lim, K.-T.; Woo, H.-S.; Park, S.-H.; Kim, Y.-R.; Kim, Y.-j.; Choung, Y.-H.; Choung, P.-H.; Chung, J.-H. Charged Nanomatrices as Efficient Platforms for Modulating Cell Adhesion and Shape. *Tissue Eng., Part C* **2012**, *18* (12), 913−923.
(38) Kizuki, T.; Ohgaki, M.; Katsura, M.; Nakamura, S.; Hashimoto, K.; Toda, Y.; Udagawa, S.; Yamashita, K. Effect of Bone-Like Layer Growth from Culture Medium on Adherence of Osteoblast-Like Cells. *Biomaterials* **2003**, *24* (6), 941−947.
(39) Guo, L.; Kawazoe, N.; Hoshiba, T.; Tateishi, T.; Chen, G.; Zhang, X. Osteogenic Differentiation of Human Mesenchymal Stem Cells on Chargeable Polymer-Modified Surfaces. *J. Biomed. Mater. Res., Part A* **2008**, *87A* (4), 903−912.
(40) Chen, H.; Fan, X.; Xia, J.; Chen, P.; Zhou, X.; Huang, J.; Yu, J.; Gu, P. Electrospun Chitosan-Graft-Poly (ε-Caprolactone)/Poly (ε-Caprolactone) Nanofibrous Scaffolds for Retinal Tissue Engineering. *Int. J. Nanomed.* **2011**, *6*, 453−461.
(41) Oyane, A.; Kim, H.-M.; Furuya, T.; Kokubo, T.; Miyazaki, T.; Nakamura, T. Preparation and Assessment of Revised Simulated Body Fluids. *J. Biomed. Mater. Res., Part A* **2003**, *65A* (2), 188−195.
(42) González-Vázquez, A.; Planell, J. A.; Engel, E. Extracellular Calcium and CaSR Drive Osteoinduction in Mesenchymal Stromal Cells. *Acta Biomater.* **2014**, *10* (6), 2824−2833.
(43) Miron, R. J.; Zhang, Y. F. Osteoinduction: A Review of Old Concepts with New Standards. *J. Dent. Res.* **2012**, *91* (8), 736−744.

(44) Vila, O. F.; Bagó, J. R.; Navarro, M.; Alieva, M.; Aguilar, E.; Engel, E.; Planell, J.; Rubio, N.; Blanco, J. Calcium Phosphate Glass Improves Angiogenesis Capacity of Poly(Lactic Acid) Scaffolds and Stimulates Differentiation of Adipose Tissue-Derived Mesenchymal Stromal Cells to the Endothelial Lineage. *J. Biomed. Mater. Res., Part A* **2013**, *101A* (4), 932−941.
(45) Aguirre, A.; Gonzalez, A.; Planell, J. A.; Engel, E. Extracellular Calcium Modulates in Vitro Bone Marrow-Derived Flk-1+ CD34+ Progenitor Cell Chemotaxis and Differentiation Through a Calcium-Sensing Receptor. *Biochem. Biophys. Res. Commun.* **2010**, *393* (1), 156−161.
(46) Laschke, M.; Harder, Y.; Amon, M.; Martin, I.; Farhadi, J.; Ring, A.; Torio-Padron, N.; Schramm, R.; Rücker, M.; Junker, D.; Häufel, J.; Carvalho, C.; Heberer, M.; Germann, G.; Vollmar, B.; Menger, M. Angiogenesis in Tissue Engineering: Breathing Life into Constructed Tissue Substitutes. *Tissue Eng.* **2006**, *12* (8), 2093−2104.
(47) Yamaguchi, T.; Chattopadhyay, N.; Kifor, O.; Butters, R. R.; Sugimoto, T.; Brown, E. M. Mouse Osteoblastic Cell Line (MC3T3-E1) Expresses Extracellular Calcium (Ca2+o)−Sensing Receptor and Its Agonists Stimulate Chemotaxis and Proliferation of MC3T3-E1 Cells. *J. Bone Miner. Res.* **1998**, *13* (10), 1530−1538.
(48) Mammoto, A.; Connor, K. M.; Mammoto, T.; Yung, C. W.; Huh, D.; Aderman, C. M.; Mostoslavsky, G.; Smith, L. E. H.; Ingber, D. E.; Mechanosensitive Transcriptional, A. Mechanism that Controls Angiogenesis. *Nature* **2009**, *457* (7233), 1103−1108.
(49) Mulder, L.; Koolstra, J. H.; den Toonder, J. M. J.; van Eijden, T. M. G. J. Relationship Between Tissue Stiffness and Degree of Mineralization of Developing Trabecular Bone. *J. Biomed. Mater. Res., Part A* **2008**, *84A* (2), 508−515.